Coupling modes of three filaments in side-by-side arrangement

Article *in* Physics of Fluids · November 2011

DOI: 10.1063/1.3659892

Coupling modes of three filaments in side-by-side arrangement

Fang-Bao Tian,[1,2,a)] Haoxiang Luo,[2] Luoding Zhu,[3] and Xi-Yun Lu[1]
[1]*Department of Modern Mechanics, University of Science and Technology of China, Anhui, Hefei 230026, China*
[2]*Department of Mechanical Engineering, Vanderbilt University, 2301 Vanderbilt Place, Nashville, Tennessee 37235-1592, USA*
[3]*Department of Mathematical Sciences, Indiana University–Purdue University Indianapolis, 402 North Blackford Street, Indianapolis, Indiana 46202, USA*

(Received 5 June 2011; accepted 14 October 2011; published online 17 November 2011)

A viscous flow past three filaments in side-by-side arrangement is studied by a numerical simulation and is accompanied by a previously established linear stability analysis. Other than the coupling modes reported previously, which include the in-phase mode, symmetrical mode, and out-of-phase mode, three additional modes are identified in the nonlinear regime by systematically varying the separation distance between the filaments. These modes are the half-frequency mode, irrational-frequency mode, and erratic flapping state. The dynamic characteristics of each mode at the saturated state is described, including the flapping amplitude, frequency, drag force, and mechanical energy of the filaments. Four typical vortex structures are observed in the wake of the filaments and are described as the coalesced vortices, symmetrical vortices, erratic vortices, and independent vortex streets. The vortex structures are closely related to the coupling modes and the dynamic characteristics of the filaments. As the Reynolds number is increased or as the bending rigidity is reduced, the filaments gain more energy and ordering of the coupling modes may change. [doi:10.1063/1.3659892]

I. INTRODUCTION

Hydrodynamic interaction of deformable bodies with the surrounding fluid is a common phenomenon, e.g., swimming fish and flapping flags. For a swimming fish, although it typically undulates its body through muscular activity for propulsion, its fins may deform passively during flapping.[1,2] Furthermore, it has been found that fish could take advantage of passive body reaction to an unsteady flow for the energy-saving purpose.[3–5] Thus, as a simple and yet useful model for understanding the role of the fluid-structure interaction in the fish behavior, flexible filaments immersed in a flow and their induced vibration have attracted significant attention since an early work by Zhang *et al*.[6]

Extensive experiments,[6–12] theoretical analyses,[13] and numerical simulations[14–17] have studied the vibration of a single filament or flag. The nondimensional mass ratio, S, defined by the ratio of the inertia of the filament to that of the fluid, is found to be a critical parameter in determining onset of the flapping motion in addition to two other dimensionless parameters involved in this problem, i.e., the flutter speed and Reynolds number. A low mass ratio tends to stabilize the filament,[10,11,18,19] and a massless filament in a uniform flow would maintain its equilibrium state even in the presence of large initial perturbations.[14] When the mass ratio is large, the filament may become unstable and develop a flapping motion.[10–12,20] The ratio of the fluid kinetic energy to the elastic energy of the filament is known as flutter speed.[7] Similar to the mass ratio, a low flutter speed tends to stabilize the filament.[9–11,16] Consequently, a filament with low bending rigidity is more likely to start the vibration. In addition, a sufficiently high Reynolds number is necessary for the flow to become unstable. The effect of the Reynolds number can be understood from the two components of the hydrodynamic force: the pressure and the shear stress. The fluid pressure can be either stabilizing or destabilizing, depending on the phase shift between the pressure and the traveling wave along the filament.[13,16] The shear stress leads to a tension in the filament, which was found to be stabilizing.[13,21,22] Since the shear stress on the filament is proportional to $Re^{-1/2}$,[23] a low Reynolds number helps to inhibit vibration of the filament.

Flow past multiple filaments placed side by side within the range of hydrodynamic interaction is an important topic in understanding the mechanism of the group behavior of the filaments. Two side-by-side filaments flapping passively in a flow were investigated experimentally by Zhang *et al*.[6] and analytically by Jia *et al*.[24] Both the in-phase and out-of-phase modes of the filaments were observed. These two modes were also captured by numerical simulations at lower Reynolds numbers.[25–27] Using a vortex method, Alben[28] observed an additional mode characterized by erratic flapping of the two filaments.

Flow-induced vibration of more than two filaments in side-by-side arrangement is less well understood. Two recent investigations on this topic are the wind-tunnel experimental measurement by Schouveiler and Eloy[29] and theoretical analysis by Michelin and Llewellyn Smith.[30] The former[29] reported that the coupling flutter modes of two, three, and four flexible plates and compared them with the modes predicted by a linear stability analysis. Three distinct coupling modes were found in the case of the three plates at the Reynolds number around 10^4: the in-phase mode, out-of-phase mode, and symmetrical mode. Their linear stability analysis

a)Author to whom correspondence should be addressed. Electronic mail: tfbao@mail.ustc.edu.cn and fangbao.tian@vanderbilt.edu.

can predict that the existence of the modes but cannot predict which mode will be selected and the observed mode in the experiment was not the mode with the largest linear growth rate. Michelin and Llewellyn Smith[30] performed an improved linear analysis for an arbitrary number of plates with the wake effect incorporated. The stability/instability regions, mode map, and growth rate were studied in detail in their work along with extensive discussions on the effects of the mass ratio, flutter speed, and separation distance. In particular, they predicted that the motion of the n identical and evenly placed plates must be symmetric or antisymmetric with respect to the symmetry plane. This interesting result is consistent to the observation in the experiment of Schouveiler and Eloy[29] for three and four plates.

To our knowledge, there is no numerical simulation done yet for more than two filaments in side-by-side arrangement. Given that there could exist complex flapping modes in the case of two filaments which cannot be predicted by linear analysis, e.g., the erratic flapping,[28] we speculate that multiple filaments may have more coupling modes than previously reported, particularly in the nonlinear regime which is beyond the scope of linear theory. Furthermore, in the two-filament setup, each filament is equivalent to the other from a symmetry point of view. However, in the setup of three or more, the inner filaments "see" a different surrounding than the outer ones, and thus they may exhibit disparate behavior. Here, we will attempt to use the three-filament configuration to gain some insight into the multi-filament systems.

In the present study, a multi-block lattice-Boltzmann method combined with an immersed-boundary method[31,32] is employed to simulate the flow over three elastic filaments in side-by-side arrangement at relatively low Reynolds numbers. A previously established linear stability analysis is also adopted here to compare with the numerical simulation. This paper is organized as follows. The physical problem and mathematical formulation are described in Sec. II. The coupling modes are presented in Sec. III. The flow characteristics are discussed in Sec. IV. The vortex structures in the flow are given in Sec. V, and finally, concluding remarks are provided in Sec. VI. The accompanying linear analysis is included in the Appendix.

II. PHYSICAL PROBLEM AND MATHEMATICAL FORMULATION

As shown in Fig. 1, three identical filaments of length L are placed side-by-side in a uniform flow with incoming velocity U_0. The separation distance between the adjacent

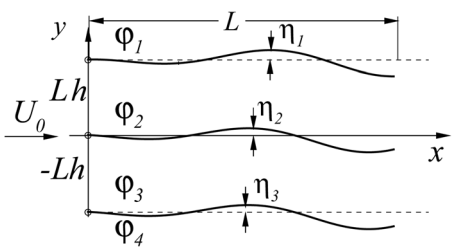

FIG. 1. Schematic of the three filaments placed side by side in a uniform flow.

filaments, normalized by L, is h. In the numerical simulation, the incompressible Navier-Stokes equations are used to describe the flow and the nondimensional forms are given by

$$\frac{\mathrm{D}\mathbf{u}}{\mathrm{D}t} = -\nabla p + \frac{1}{Re}\nabla^2\mathbf{u} + \mathbf{b}, \quad \nabla\cdot\mathbf{u} = 0, \tag{1}$$

where $\mathbf{u} = (u,v)$ is the fluid velocity, p is the pressure, $\mathbf{b} = (b_x, b_y)$ is the body force, D/Dt is the material derivative, and Re is the Reynolds number. All the variables have been scaled using the fluid density ρ, U_0, and L. The normalized governing equation for the dynamics of each filament in the two-dimensional plane is[14,15,31]

$$S\frac{\partial^2\mathbf{X}}{\partial t^2} - \frac{\partial}{\partial s}\left[T(s)\frac{\partial\mathbf{X}}{\partial s}\right] + U^{-2}\frac{\partial^4\mathbf{X}}{\partial s^4} = \mathbf{F}_f, \tag{2}$$

where $\mathbf{X}$ is the position vector of a point on the filament, s is the arc length along the filament, $T(s) = K_s\left(\left|\frac{\partial\mathbf{X}}{\partial s}\right| - 1\right)/(\rho U_0^2 L)$ is the in-plane tension, $\mathbf{F}_f$ is the hydrodynamic traction per unit length of the filament, S is the mass ratio defined by $S = m_s/\rho L$, and U is the flutter speed defined by $U = \sqrt{\rho U_0^2 L^3/E_b}$. Here m_s, K_s, and E_b are the linear density, stretching coefficient, and bending rigidity of the filament, respectively. The stretching coefficient is sufficiently large so that the filaments are nearly inextensible.

The modified penalty immersed-boundary method coupled with a lattice-Boltzmann method[31,32] is adopted to solve the fluid-structure interaction problem. In this approach, the kinetics of the fluid is governed by the discrete lattice-Boltzmann equation of a single relaxation time model,[33–35] and the multi-block lattice-Boltzmann method proposed by Yu, Mei, and Shyy[36] has been incorporated. The fluid–solid boundary is handled by a modified version of the penalty immersed-boundary method originally developed by Kim and Peskin.[37] In this immersed-boundary method, the no-slip boundary condition is achieved by including a body force component, $\mathbf{b}$, in the momentum Eq. (1) with

$$\mathbf{b}(\mathbf{x},t) = -\sum_{i=1}^{3}\int_{s_i}\mathbf{F}_f(s,t)\delta(\mathbf{x} - \mathbf{X}(s,t))ds, \tag{3}$$

where i represents the ith filament and $\delta(\mathbf{x} - \mathbf{X}(\mathbf{s}, t))$ is Dirac's delta function. In the numerical method, the delta function is replaced by a smooth approximation adopted by Shi and Phan-Thien.[38] The speed of the filament is interpolated from the flow field onto the Lagrangian points discretizing the filament, and the position of those points is updated by explicitly integrating the velocity. A finite-difference method is used to calculate the second and third terms on the left-hand side of Eq. (2). To calculate the inertial force term in Eq. (2), the penalty method used in Kim and Peskin[37] is adopted to ensure the numerical stability. Specifically, the filament itself is assumed to be massless in the algorithm, but a ghost filament of linear density m_s is attached to the physical filament through a spring of specified stiffness. The inertial term in Eq. (2) is thus replaced by the spring force. The physical contact between adjacent filaments is not modeled here. Fortunately, the contact or overlapping does not

happen in our simulation, likely due to the relatively low Reynolds number considered. The details of the algorithm and its validation can be found in our previous work.[31,32]

In the present study, we will mainly focus on the effect of h on the dynamic characteristics. The effects of Re and U will be discussed briefly in the end. For the baseline simulation, we choose $Re = 100$, $S = 0.3$, and $U = 10$. As previous numerical studies of flapping filaments,[15,25,39] low Reynolds numbers (in comparison with that in the experiment of Schouveiler and Eloy[29]) are adopted here to reduce the simulation cost. The normalized stretching coefficient, $K_s/(\rho U_0{}^2 L)$, is $O(10^3)$ to make sure that the filament extension is small and meanwhile the simulation is stable. To induce the onset of instability in the simulations, we introduce a small-amplitude, sinusoidal perturbation to the initial state of the filaments while keeping the filament length unchanged.

III. COUPLING MODES

In this section, we present the flapping modes of the filaments observed in the numerical simulations and compare the modes with predictions by linear theory given in the Appendix.

A. In-phase mode at small *h*

In the linear analysis outlined in the Appendix, one solution of $|\mathbf{M}| = 0$ in Eq. (A5) requires

$$\eta_{03}/\eta_{01} = 1, \eta_{02}/\eta_{01} = -a/c = -2c/b = \gamma, \tag{4}$$

where γ takes one of two values

$$\gamma_1 = (-e^{-kh} - \sqrt{e^{-2kh} + 8})/2,$$
$$\gamma_2 = (-e^{-kh} + \sqrt{e^{-2kh} + 8})/2. \tag{5}$$

Note that γ_1 and γ_2 have opposite signs. If $\gamma = \gamma_1$, then the inner filament is out of phase with the outer filaments, and if $\gamma = \gamma_2$, then all three filaments are in phase, which is labeled with M1. In particular, as $h \to 0$, we have $\gamma_2 = 1$, meaning that all the filaments have the same amplitude as well. In this case, substituting the amplitude ratios into Eq. (A5) and then adding the three component equations, we obtain

$$(\omega + k)^2 + [(3S)\omega^2 k - (3U^{-2})k^5]/2 = 0, \tag{6}$$

which is the same as the corresponding equation for a single filament perturbed in a freestream,[9] except that S and U^{-2} here have been multiplied by a factor of 3. Theoretically, the assembly of three filaments behaves like a single filament with the mass and bending stiffness tripled. Therefore, the in-phase mode at small h is further termed the single-filament mode here or M1a. The nonlinear dynamics of this mode will be later compared with the in-phase mode at large h.

The single-filament mode is confirmed by our numerical simulation. Fig. 2 shows the vorticity contours and the displacement of the filament tails versus time at $h = 0.1$, where y_L is defined as $y_L = y(L) - y(0)$ with $y(0)$ and $y(L)$ being the y-coordinates of the head and tail of the filament, respectively. It is identified that the three filaments flap in phase as

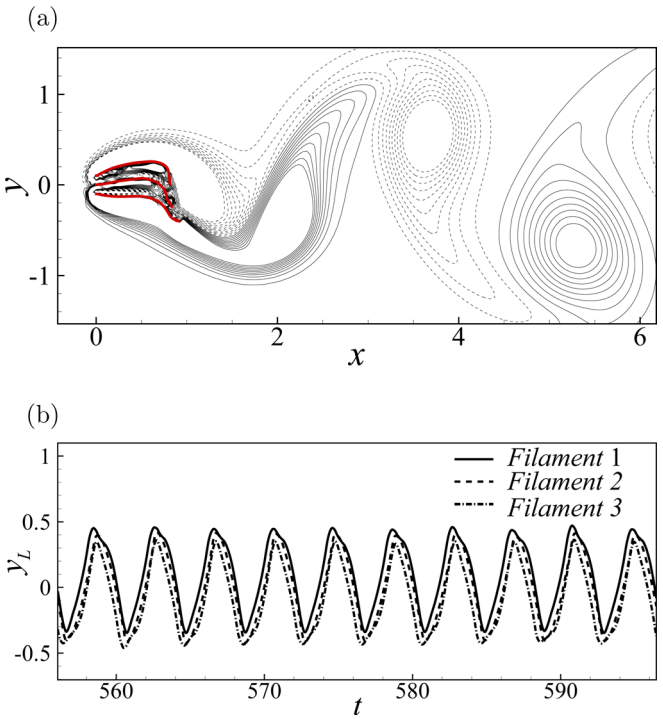

FIG. 2. (Color online) The single-filament mode (M1a) of the three filaments at $h = 0.1$: (a) the vorticity field and (b) the displacement of the tails as a function of time.

a single one and the vortex street is similar to that of a single filament in a uniform flow (Fig. 2(a)). Complementary simulations show that even if the filaments in this case did not start from the in-phase configuration initially, they also quickly settle down to the single-filament mode after several cycles. Fig. 2(b) shows that the oscillations of the three filaments are nearly periodic and the difference among the oscillation amplitudes is small (less than 3%). Note that the flapping amplitude in the simulation is beyond the limit of linear theory. In addition, it is noticed that the oscillations of the two outer filaments are slightly biased while that of the inner filament is nearly symmetric about $y = 0$. This single-filament mode was also found in the two parallel filaments[6,24,25] and three parallel plates.[29,30]

B. Symmetrical mode

Another solution to $|\mathbf{M}| = 0$ in Eq. (12) is $a = 0$, which requires $\eta_{02} = 0$ and $\eta_{01} = -\eta_{03}$. For this mode, the inner filament remains a straight line along the x-axis, while the two outer filaments flap in the opposite phase. This is the symmetrical mode reported previously[29,30] and is labeled with M2 here. The vorticity field and the tail displacement of the three filaments at $h = 0.4$ are plotted in Fig. 3. The instantaneous filament deformation and the vorticity field during the established state are shown in Fig. 3(a). It is observed that both the filaments and flow field are symmetric about the center line of the domain. Moreover, the average positions of the two outer filaments are not in parallel with the x-axis any more, and their tails on average may point outward. A similar flow field to the current mode was also observed in the corresponding cases of two filaments.[6,25,39] As shown in Fig. 3(b), the three filaments settle down to this mode after a

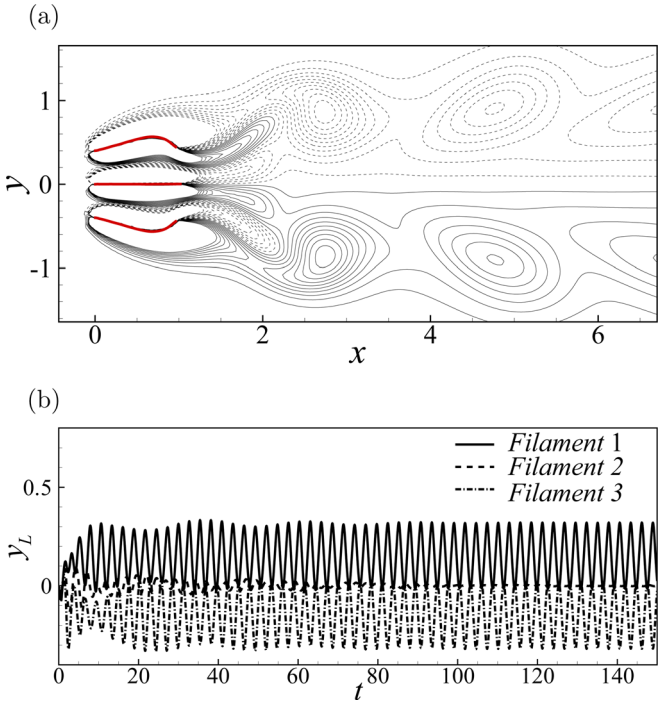

FIG. 3. (Color online) The symmetrical mode (M2) of the three filaments at $h = 0.4$: (a) the vorticity contours and (b) the displacement of the tails as a function of time.

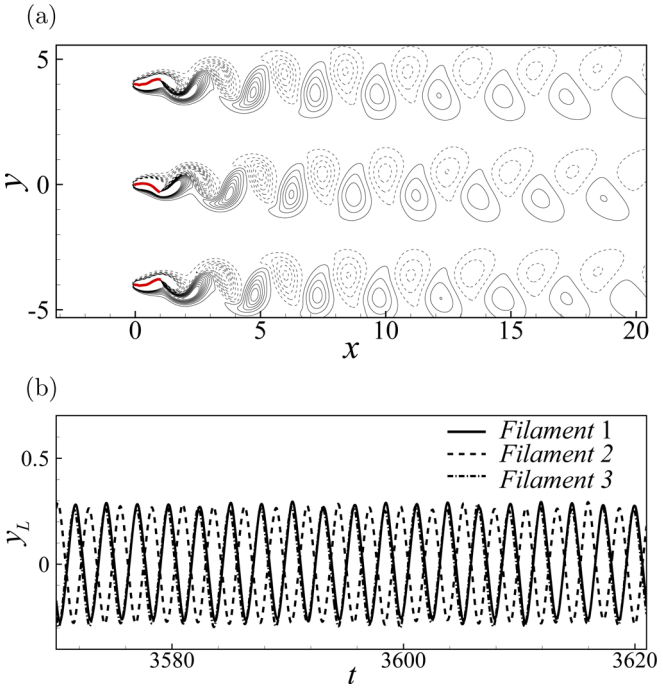

FIG. 4. (Color online) The out-of-phase mode (M3) of the three filaments at $h = 4.0$: (a) the vorticity field and (b) the tail displacement of the filaments as a function of time.

transition period around $t < 80$ (the initial perturbation to the filaments' deflection in this case was an in-phase configuration).

C. Out-of-phase mode

In Eq. (5), if $\gamma = \gamma_1$, the filaments display an out-of-phase mode that has been reported previously[29,30] and is labeled here with M3. This mode is observed in our numerical simulation at $h = 4.0$ and is shown in Fig. 4. Fig. 4(a) shows that an independent vortex street is formed behind each filament. The two outer filaments are in phase with each other and so are the vortices behind them. The inner filament is out of phase, and the vortices behind it have opposite signs compared to the other vortices at the same streamwise location.

Moreover, Fig. 4(b) shows that all three filaments have almost the same vibration amplitude. This is different from the prediction of linear theory, as Eq. (4) would give $\eta_{03} = \eta_{01}$ and $\eta_{02} = -\sqrt{2}\eta_{01}$, meaning that the inner filament would have a much higher vibration amplitude. The discrepancy is understandable since linear analysis is only valid for small-amplitude deformations while the numerical simulation captures the saturated nonlinear vibration.

D. In-phase mode at large *h*

As shown in Michelin and Llewellyn Smith,[30] the dominating coupling modes may appear alternately when h is varied continuously. This pattern is also found in the nonlinear regime by the present simulation. However, as h becomes large enough, the interaction among the filaments is expected to be weak. For a two-filament setup, Alben[28] found that the interaction still exists when h is more than 10. Here, we have seen significant interaction for h up to 15. As shown in Fig. 5, the coupling among the filaments at $h = 15$ is still strong enough to cause a coordinated vibration. The simulation was started with the inner filament having an out-of-phase deformation with the outer filaments. It is seen that during the first 25 cycles the vibration amplitudes of the filaments have grown to their full potential, but their relative phases remain unchanged. After a long period of adjustment, the system settles down to an in-phase mode in which the filaments exhibit nearly sinusoidal oscillations. A similar transition process is generated when different initial configurations are used. This in-phase mode is thus similar to the single-filament mode, M1a, that happens at small h and the two should belong to the same mode in the linear regime. However, the wake of the filaments is quite different from that of the single-filament mode, and an independent vortex street is formed here behind each filament. This mode is thus labeled with M1b.

E. Half-frequency mode

In addition to the in-phase, symmetrical, and out-of-phase modes that have been previously reported for multiple filaments, three more coupling modes have been identified here in our simulations. The first one is observed when the separation distance is between those for M1a and M2, named the half-frequency mode or M4. A specific example of M4 is shown in Fig. 6 for $h = 0.2$. In this mode, the two outer filaments flap with the same frequency and are nearly out of phase, while the inner filament flaps at a reduced frequency that is only half that of the outer filaments. As shown in Fig. 6, this mode is established after a transition period which is more than 800 time units. During the transition, the

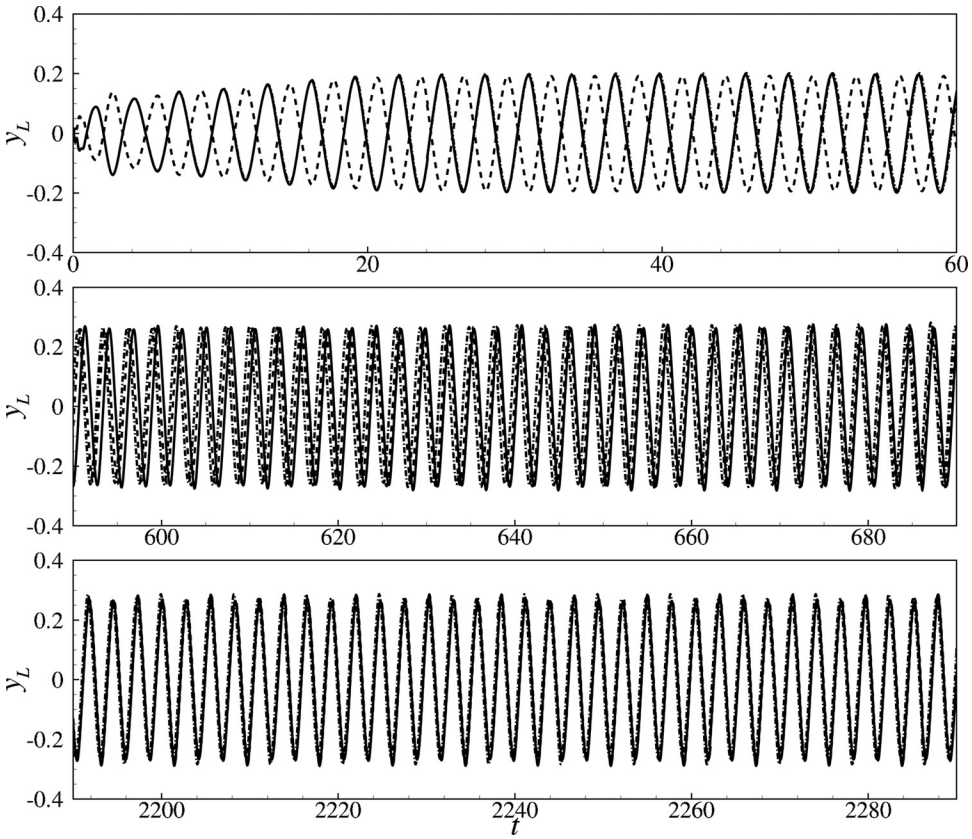

FIG. 5. The in-phase (M1b) at $h = 15.0$: the tail displacement of the three filaments during the start (top), transitional (middle), and established (bottom) periods (see previous figures for the legends).

inner filament flaps at the halved frequency, but the flapping amplitude varies irregularly. Thus, this filament exhibits an intermittent fluttering behavior at early stage. The entire simulation was run up to $t = 2000$ to ensure that the final mode is sustained. During the stationary vibration, it is seen from the history of the tail displacement that the three filaments come together every time when the inner filament reaches its maximum excursion on either side. Thus, a full cycle of the outer filaments corresponds to a half cycle of the inner filament. Furthermore, the two consecutive cycles of each outer filament are clearly different due to the interference of the inner filament. When the inner filament moves toward one side, the outer filament on that side may experience less deformation, while the filament on the other side may subject to more deformation. Therefore, both the outer filaments alternate between a smaller-amplitude cycle and a larger-amplitude cycle.

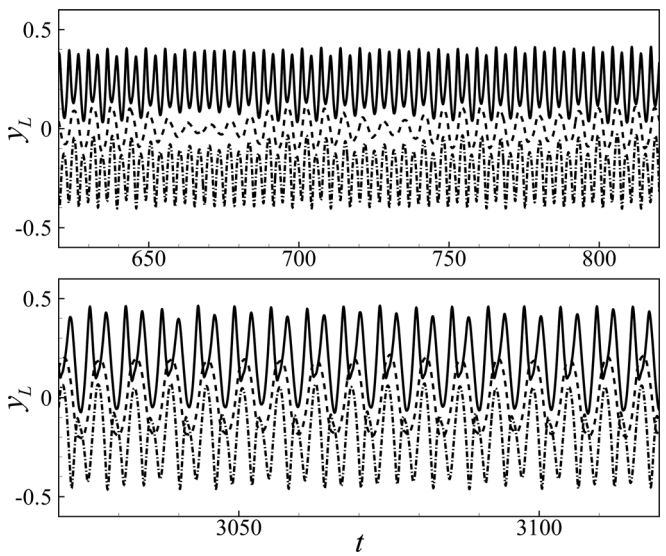

FIG. 6. The half-frequency mode (M4) of the three filaments at $h = 0.2$: the tail displacement of the filaments 1 (solid line), 2 (dashed line), and 3 (dashed-dotted line) during the transitional period (top) and established period (bottom).

F. Irrational-frequency mode

The second new mode observed here is within the interval of $1.25 < h < 3.2$ and is named as the irrational-frequency mode or M5. For this mode, the three filaments vibrate at a similar amplitude. However, the frequency of the inner filament is slightly different from those of the outer filaments. Fig. 7(a) shows the tail displacements of the three filaments at $h = 2.5$. It is observed that the inner filament flaps around one more cycle than the outer filaments in the shown time window. The corresponding power spectrum density (PSD) of the tail displacement in Fig. 7(b) further demonstrates the frequency difference between the inner filament and the outer filaments. The phase difference between the outer filaments, even though not strictly a constant, is nearly π in most of time; it means that the two filaments are generally out of phase with each other. From a symmetry perspective, both the half-frequency and irrational-frequency modes can be viewed as a result of an unstable symmetrical mode, where the instability of the inner filament destroys the instantaneous symmetry of the three filaments. Furthermore,

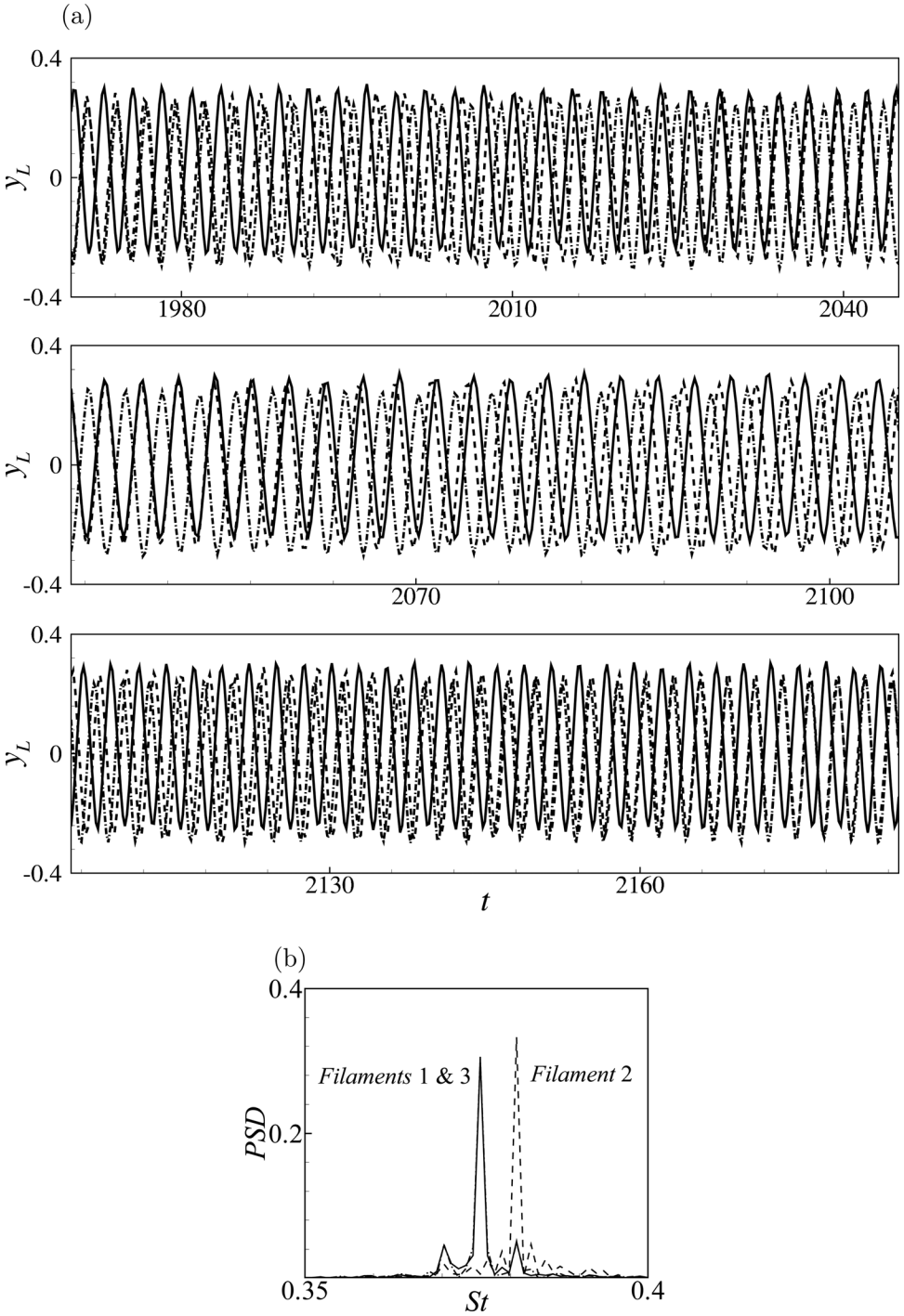

FIG. 7. The irrational-frequency mode (M5) of the three filaments at $h = 2.5$: (a) the tail displacement of the filaments 1 (solid line), 2 (dashed line), and 3 (dashed-dotted line); (b) the PSD of the tail displacement vs the reduced frequency, $St = fL/U_0$.

the inner filament displays a bifurcation behavior that it tends to follow either of the outer filaments in its oscillation.

G. Erratic flapping

In addition to the five coupling modes described above, we also found that, between the symmetrical mode (M2) and the irrational-frequency mode (M5) and approximately in the region of $0.5 \leq h \leq 1.0$, there is an erratic flapping state in which the frequency and amplitude of the filaments vary irregularly with time. An example is shown in Fig. 8 for $h = 0.6$. The current erratic flapping phenomenon is similar to that of two parallel filaments at the separation distance $h < 1.0$ studied by Alben.[28] He found that the two filaments flap nearly in phase in some time intervals, more often nearly out of phase in some other time intervals, and some time with one filament having much larger amplitude than the other. Such an erratic behavior is also observed in the present three-filament system but mainly in the two outer filaments. As shown in Fig. 8 (and also a closeup view in Fig. 13(i)), the vibration of the inner filament is relatively consistent. However, the amplitude of each outer filaments appears to be modulated by another oscillatory wave with a lower frequency. Furthermore, the modulating waves of the outer filaments have a phase difference. Therefore, filaments 1 and 3 alternately experience a short period of an inactive state every few cycles before starting to flap normally. Along with the

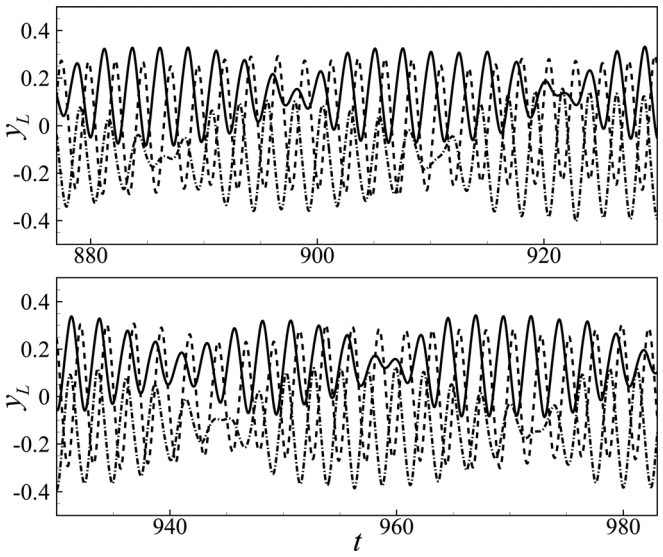

FIG. 8. The erratic flap of the three filaments at $h = 0.6$: the tail displacement of the filaments 1(solid line), 2(dashed line), and 3(dashed-dotted line).

amplitude variation, there is also a phase variation among the filaments; the figure shows that at some time filaments 1 and 2 are out of phase and at some other time filaments 3 and 2 are out of phase.

IV. CHARACTERISTICS OF THE FLOW-STRUCTURE INTERACTION

In this section, we will discuss the flapping amplitude, frequency, drag force, and mechanical energy of the three filaments for each coupling mode and will discuss the relationships among these quantities.

A. Flapping state and drag force

We first quantify the flapping amplitude defined by the root-mean-square (RMS) value of the deflection of the free end, the normalized flapping frequency defined by $St = fL/U_0$, and the drag for each one of the three filaments, where f is the flapping frequency. Fig. 9 shows the normalized amplitude A/A_0, St, and time-averaged drag $C_D/C_{D,0}$ of each filament versus h, where A_0 and $C_{D,0}$ are, respectively, the amplitude and averaged drag for a corresponding single filament vibrating in a free-stream.

It is seen from Fig. 9(a) that the amplitudes of the two outer filaments are very close to each other, which is expected due to the symmetric configuration of the problem. The amplitude of the inner filament is significantly different from that of the outer filaments, in particular at the interval of $0.15 < h < 1.5$. Later we will further discuss the behavior of the inner filament in conjunction with the vortex dynamics. At $h = 0.1$, the amplitude of each filament is increased by 40% compared to that of a single filament. This behavior may be understood by the fact that the closely separated filaments flap as if they were a single filament with tripled mass and rigidity and a single filament of higher mass ratio is known to flap more violently compared to a corresponding filament of lower mass ratio.[9,11,16]

In $0.15 \leq h \leq 1.5$, the amplitude of the filaments, especially the outer filaments, is significantly reduced. This reduction of vibration can be attributed to the frequency and

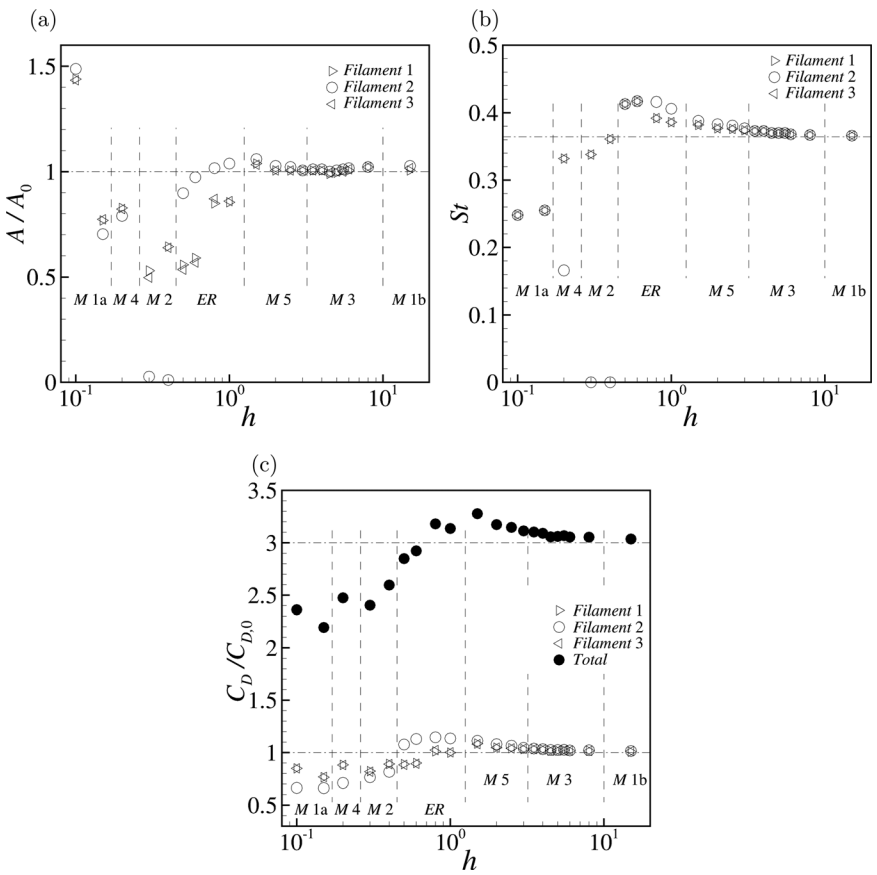

FIG. 9. The time-averaged (a) vibration amplitude, (b) frequency, and (c) drag versus h for the three-filament system. The coupling modes are, in their order, the in-phase single-filament mode (M1a), half-frequency mode (M4), symmetric mode (M2), erratic flapping (ER), irrational-frequency mode (M5), out-of-phase mode (M5), and in-phase mode at large h (M1b).

phase differences among the filaments. For example, even though the case at $h=0.15$ belongs to the single-filament mode and the three filaments on average have the same frequency as shown in Fig. 9(b), there is a small amount of phase difference that changes with time among the filaments due to the frequency variation. The asynchronization prohibits the filaments at close separations from vibrating with a large amplitude because the space is limited and the filaments cannot cross over each other. A similar reasoning also applies to the half-frequency mode (M4), the symmetric mode (M2), and the erratic flapping mode where h is relatively small. For the irrational-frequency mode (M5) and out-of-phase mode (M3), the distance among the filaments is large, and the phase difference has less effect on the vibration amplitude. For these modes and also the in-phase mode M1b, the amplitudes of the three filaments are all close to that of a single filament.

Fig. 9(b) shows the normalized flapping frequency of each filament, St, averaged in time for each coupling mode. Note that the instantaneous frequency of the filaments may vary slightly. The averaged frequencies of the outer filaments are the same in all cases, but that of the inner filament may be significantly different, as in the half-frequency mode, symmetrical mode, and irrational-frequency mode. At $h=0.1$, the frequency of the outer filaments is $St=0.25$, which is much lower compared to that of a single filament, $St=0.36$. Overall, as h is raised, the frequency of the outer filaments first increases and then reaches its maximum near $h=0.7$, where St for the erratic flapping is 10%–14% larger than that of the single filament. In addition, from M1a to M4, there is a frequency jump, where the frequency of the inner filament suddenly drops while the frequency of the outer filaments rises. As h is increased beyond 0.7, the flapping frequency approaches gradually to that of a single filament.

Both the drag of each filament and the total drag of the three filaments are plotted in Fig. 9(c). The overall trend of the total drag is similar to that of the flapping frequency of the outer filaments shown in Fig. 9(b). The total drag is lower for the single-filament mode and increases initially as h becomes larger. For $h<0.7$, the total drag is less than $3C_{D,0}$. The total drag becomes higher and above $3C_{D,0}$ when h is between 0.7 and 3. As h is further increased, the total drag approaches to the drag of three independent filaments. Note that at $h=0.1$, even though each filament has an augmented vibration amplitude, the frontal areas of the three filaments overlap with each other due to the close separation and the in-phase deformations. Thus the total drag actually falls much below $3C_{D,0}$. Furthermore, each individual filament enjoys a drag reduction through the cooperated vibration. The reduction is more than 40% for the inner filament and more than 10% for the outer filaments.

B. Mechanical energy of the filaments

The filaments sustain their vibration by exchanging energy with the surrounding fluid. The energy flow is two-directional; it means that each filament may both extract and release energy in a vibrational cycle, depending on the phase stage in the cycle. The net energy flow is zero once the filaments establish their vibration since the physical damping of the filaments is set to be zero. The mechanical energy of each filament can be further divided into the elastic potential due to the deformation, E_p, and the kinetic energy, E_k, which are defined as

$$E_p(t)=\frac{1}{2U^2}\int\left|\frac{\partial^2\mathbf{X}}{\partial s^2}\right|^2 \mathrm{d}s,$$
$$E_k(t)=\frac{S}{2}\int\left|\frac{\partial\mathbf{X}}{\partial t}\right|^2 \mathrm{d}s. \tag{7}$$

Note that the elastic potential due to stretching is excluded from the calculation because it is at least one order of magnitude lower than the bending energy.

The time-averaged elastic potential and kinetic energy are shown in Fig. 10(a) for filaments 1 and 2, and in Fig. 10(b) for the three filaments together. For an individual filament, the averaged elastic potential is not necessarily equal to the averaged kinetic energy. For example, in M1a, M4, and M2, E_p is generally higher than E_k, while for erratic flapping, E_k can be significantly higher than E_p. Comparing the outer filaments with the inner filament, we notice that for M1a, the outer filaments have significantly higher energy than the inner filament at small separation but have lower energy when the separation is somewhat increased. For M4 and M2, the inner filament flaps at a half frequency or remains largely still. Thus, it sustains lower energy

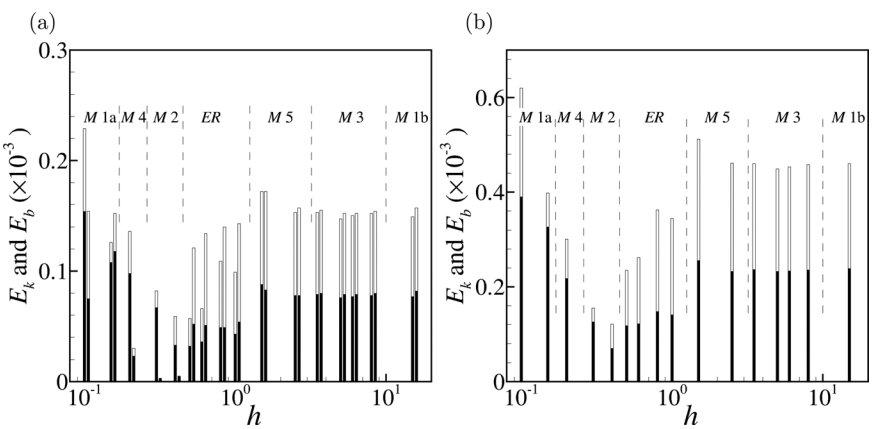

FIG. 10. The time-averaged elastic potential (black bar) and kinetic energy (white bar) for selected cases in each mode. (a) Energies for filament 1 (left) and filament 2 (right); (b) total energy of the three filaments.

compared to the outer filaments. For the erratic flapping, the inner filament has higher energy since its vibration amplitude is larger with respect to the outer filaments. For the rest modes where h is large, all three filaments have nearly the same amount of energy. In addition, at $h > 2$, each filament's energy is approximately equal to that of the single filament in a uniform flow.

The total energy of the three-filament system also displays substantial variations as the separation distance and the coupling mode are altered. There is clearly a low energy zone between $h = 0.2$ and $h = 1$ that covers M4 and M2 as well as the erratic flapping. The total energy is only higher than 3 times the energy of the single filament for some of the cases in M1a and M5.

C. Effects of the Reynolds number and bending rigidity

Michelin and Llewellyn Smith[30] carried out an extensive study of the effects of the mass ratio and bending rigidity on the coupling modes of three filaments. They showed that these parameters have strong influence on the ordering of the modes as h is varied. Due to the cost of simulations, we are not able to perform a similar parametric sweep. Nevertheless, limited study is done here to show that the Reynolds number and bending rigidity could affect the mode ordering in the nonlinear regime as well.

For an elastic and slender structure, e.g., a filament or a plate, suspended in a free-stream with the upstream end anchored, increasing either the mass ratio or the Reynolds number produces a destabilizing effect and may lead to the onset of the flow-induced vibration.[9,16] On the other hand, the bending rigidity of the structure plays a stabilizing role. For multiple structures placed in parallel in a flow, the structures may remain stable within a certain parameter regime, such as the Reynolds number being low enough. It is expected that if the Reynolds number or the mass ratio is increased, or if the bending rigidity is decreased at this point, the structures may become unstable and start to flap at certain coupling mode. Further change of these parameters may cause the structures to gain more energy and alter their vibration mode. To verify this character, we have performed a series of simulations by setting $h = 0.4$ and varying the Reynolds number from 60 to 200. The other parameters are the same as in the baseline configuration. In these tests, the three filaments are stable as $Re \leq 80$. When $80 < Re < 110$, the three filaments flap in mode M2, where the inner filament is stable and the outer filaments are out of phase. The filaments enter mode M3 as $110 \leq Re < 150$ and then to the erratic flapping state when $Re \geq 150$. As Re is raised to 150 for the cases in Fig. 9, M2 disappears from the mode spectrum, and M3 appears in the region between M4 and the erratic flapping. Furthermore, both the energy level of the filaments and energy exchange between the filaments and the fluid become higher as Re is raised.

To see how the elasticity of the filaments changes the vibration mode, we doubled the bending rigidity in the baseline configuration and repeated the simulations for a range of h. The result shows that M4 disappears from the mode spectrum and mode M2 extends to a lower h. Meanwhile, both the energy level of the filaments and energy exchange between the filaments and the fluid are reduced. The change of the coupling mode with the bending rigidity can also be seen from the experimental study of Schouveiler and Eloy[29] for three flexible plates with $h = 0.137$ and $S = 1.43$. In their work, when the flutter speed is $U = 8.4$, the three plates flap with a mode similar to M2 in the present study. When the flutter speed is increased to $U = 14.26$, the plates flap with a mode similar to M1a here.

V. VORTEX STRUCTURES IN THE WAKE

The vortex structures in the wake of multiple bodies are closely related to the coupling modes of the bodies. The examples include rigid bodies mounted on elastic foundations[40] and deformable thin structures like filaments and plates.[6,25,39,41] In our simulations, we have identified four types of vortex structures that are associated with the coupling modes of the filaments and will discuss them in this section.

A. Coalesced vortex structures

The vortex coalescence happens in both the near- and far-field wakes. For mode M1a, the coalescence occurs immediately next to the free ends of the filaments, as shown in Fig. 2(a) for the instantaneous vorticity contours. It is noticed that the vortex structure is the similar to those of a single filament at moderate Reynolds number[14,15,31,39] and two parallel filaments at close range.[25,39] Because of the small separation, the vortices generated in the gaps between filaments 1 and 2 (or between filaments 2 and 3) coalesce into the negative vortices generated from the upper surface of filament 1 (or the positive vortices generated from the lower surface of filament 3). The positive and negative vortices shed alternately into the wake forming a strong Kármán vortex street, which induces the violent flapping of the filaments. Therefore, the amplitude and mechanical energy of the filaments in this mode are the largest in comparison with the other modes, as shown in Figs. 9 and 10.

For mode M4, coalescence of vortices occurs in the far-field wake. Fig. 11 shows the typical process of such coalescence. When the tails of the two outer filaments are bent inward (Figs. 11(a) and 11(b)), a positive vortex is formed near filament 3, which is marked as V_3. There are two other positive vortices downstream filament 3 that are formed in the earlier cycles and are marked as V_1 and V_2 in the figure. As filament 3 is bending outward, vortex V_3 is further developed, as shown in Figs. 11(c) and 11(d). Meanwhile, vortices V_1 and V_2 are convected downstream and begin to merge. As filament 3 is bending inward again, V_3 is pinched off from filament 3, while V_1 and V_2 have merged with each other (Figs. 11(e) and 11(f)). Then, two subsequent positive vortices, V_3 and V_4 shed from filament 3, will also merge together into a large vortex (Figs. 11(g) and 11(h)). Similarly, each two vortices shedding from filament 1 will merge into one negative vortex. The merged positive and negative vortices alternate in their location and form a single Kármán vortex

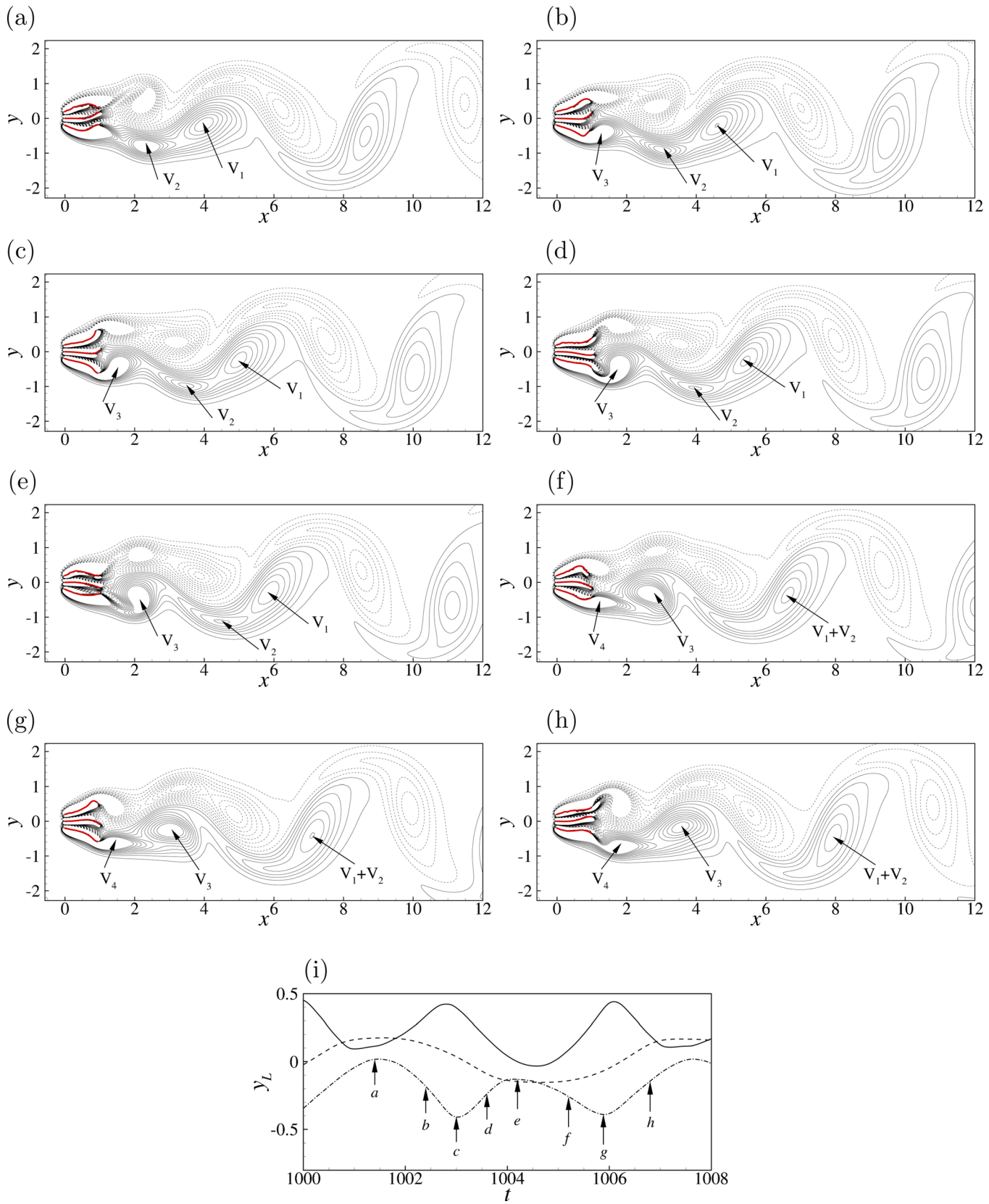

FIG. 11. (Color online) The instantaneous vorticity fields for mode M4 at $h = 0.2$ (a)-(h). The corresponding time stamps are indicated in (i), where the tail displacement is plotted for filaments 1 (solid line), 2 (dashed line), and 3 (dashed-dotted line).

street downstream the three filaments. Moreover, the frequency of the vortex merging is half of the flapping frequency of the outer filaments and, interestingly, it corresponds to the flapping frequency of the inner filament. Therefore, it is possible that the far-field vortices have caused the low-frequency flapping of the inner filament.

B. Symmetric vortex structures

Symmetric vortex structures in the wake of the filaments are found in M2 where the filaments vibrate symmetrically about the center line. Fig. 12 shows the instantaneous vorticity contours. An important feature of this wake is that the vortex structures tend to dissipate more quickly compared to those in the other modes, e.g., M1a and M3. To explain the phenomenon, we notice that major vortex shedding takes place at filaments 1 and 3 when they are bending outward. When these two filaments are bending inward, there are small vortex pairs formed in the gap regions between two adjacent filament pairs, i.e., filaments 1 and 2, and filaments 2 and 3, which are indicated in Fig. 12(a). These vortex pairs are convected downstream, merge into the vortex street from the outer sides of filaments 1 and 3, and thus weaken the large vortex (see Fig. 12). Since vortex shedding mainly occurs as the filaments bend outward, the wake of filament 1 contains only negative vortices, and the wake of filament 3 contains only positive vortices.

The wake dissipation can also be understood from the vortex dynamics theory.[42,43] Since the vorticity dissipation is directly associated with the enstrophy dissipation rate ϕ_ω, $\varphi_\omega = \nabla\boldsymbol{\omega} : \nabla\boldsymbol{\omega}/Re$, existence of a large gradient in the vorticity field will lead to stronger dissipation. The close distance between the large vortices and the small vortices of opposite signs creates such a large vorticity gradient, and thus the vortex dissipation is accelerated. We have calculated the enstrophy dissipation rate in the simulation and found that ϕ_ω in M2 in the near-field wake is several times higher than that in M1a and M3. Thus, it is not surprising that the vortex street in those modes can maintain its structure up to a long distance downstream the filaments. Corresponding to the weak vortex structures, the flapping amplitude and mechanical energy of M2 are much lower than those of the other modes.

C. Erratic vortex structures

Fig. 13 shows a sequence of vorticity field for the erratic flapping state at $h = 0.6$. Similar to the symmetrical mode shown in Fig. 12, the inner filament does not have a well-established vortex street of its own, and the wake of the outer filaments contains only vortices of the same sign. However, the dynamical behavior of the vortices are more complex in the erratic flapping. Combining the vorticity field in Figs. 13(a)–13(c) and the corresponding deflection of the filaments, we notice that the phase difference between filaments 2 and 3 is changing from π to approximately $\pi/2$ and that the positive vortices shedding from filament 2 tend to diminish the negative vortices and strengthen the positive vortices shedding from filament 3. As a result, the vibration amplitude of filament 3 is enhanced. On the other hand, filament 1 during this period is experiencing a suppressed vibration. However, it is nearly out of phase with filament 2, and its vibration is being enhanced.

Following a few cycles of transition, the vibration of filament 3 is suppressed, while filament 1 is flapping with its maximum amplitude. The vortex structures at this stage are shown in Figs. 13(d)–13(f). It is seen that the relative phase between filaments 1 and 2 has shifted and approaches to $\pi/2$. Meanwhile, the negative vortices shedding from filament 2 tend to diminish the positive vortices and strengthen the negative vortices shedding from filament 1. In the subsequent cycles as shown in Figs. 13(g)–13(h), the vibration of filament 1 has decreased, and filament 3 has adjusted its phase to be opposite to that of filament 2 and has started to grow again. Throughout the process, the inner filament maintains a relatively consistent flapping motion, while the outer filaments go through the alternating inhibited and enhanced flapping states.

D. Independent vortex streets

As the separation between the filaments becomes large, e.g., $h > 1.25$, the vortex structure behind each

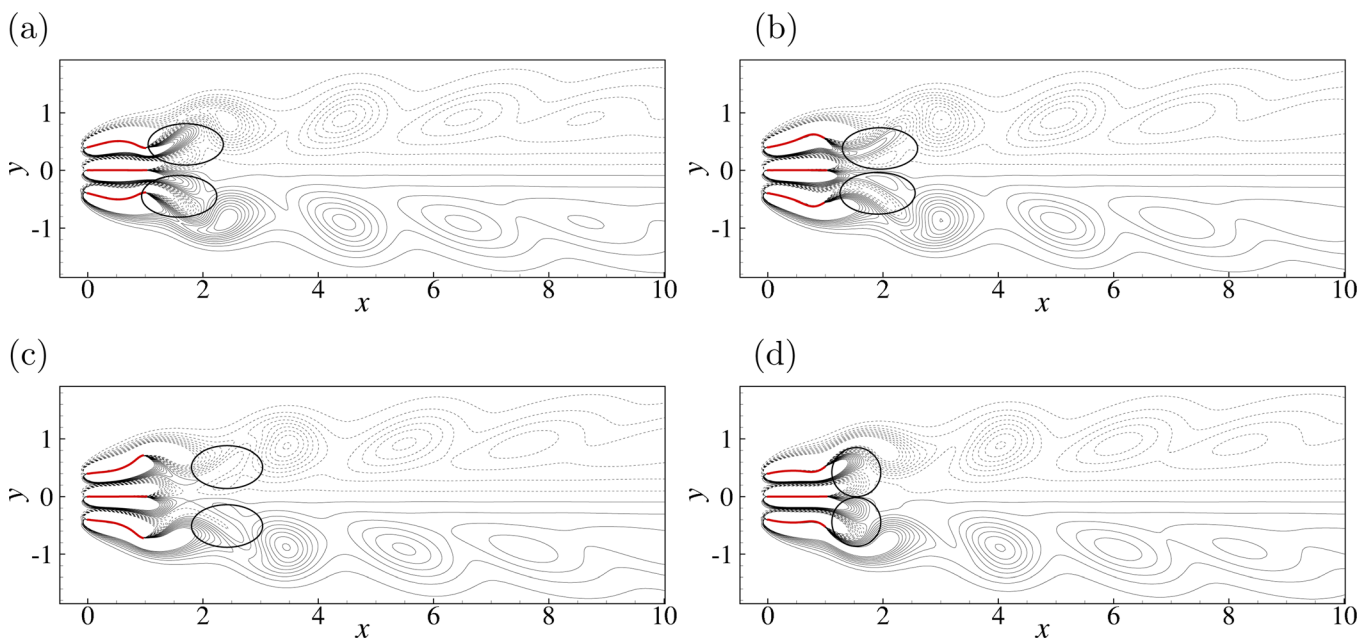

FIG. 12. (Color online) The instantaneous vorticity field within one cycle for M2 at $h = 0.4$.

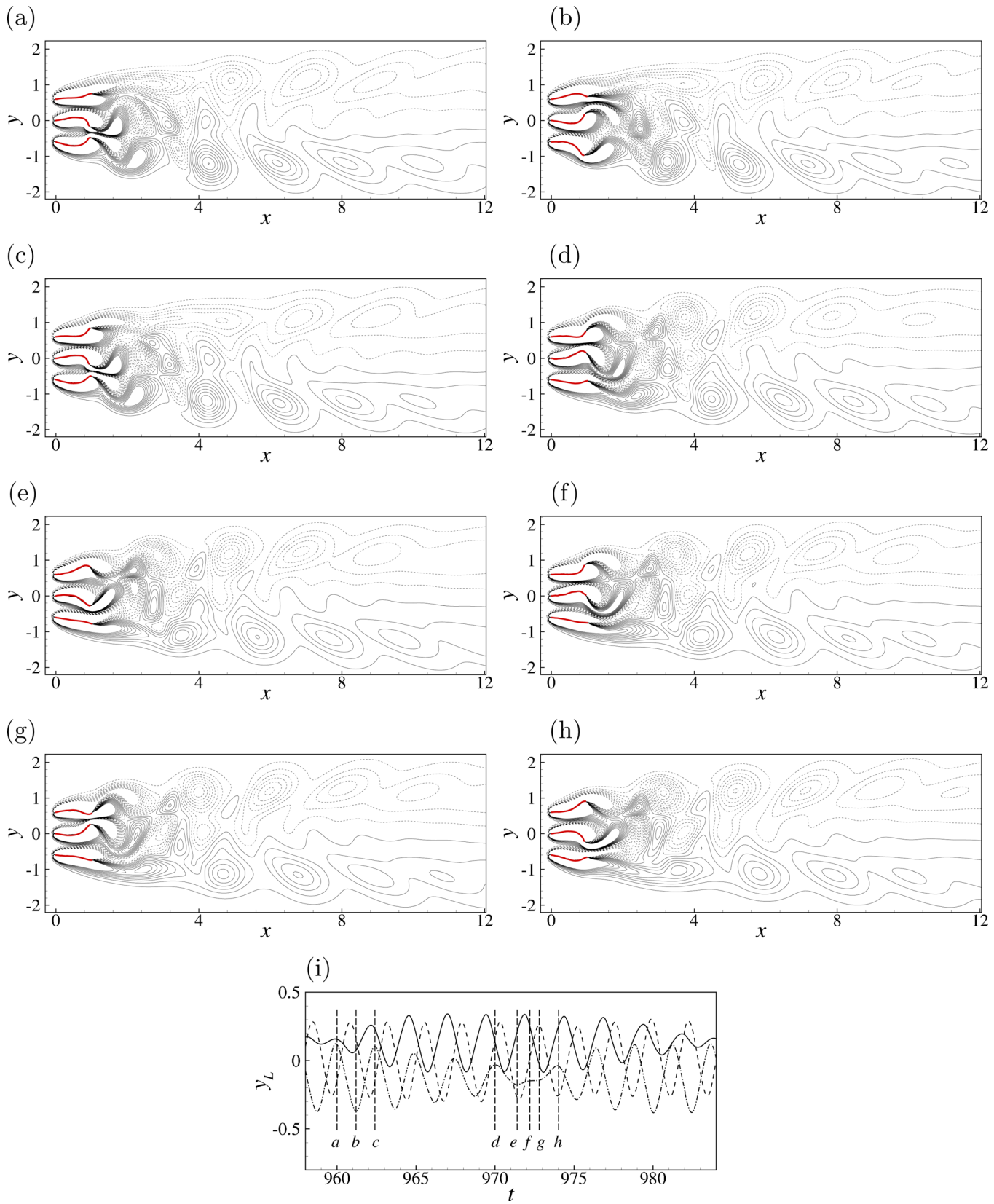

FIG. 13. (Color online) The instantaneous vorticity field for ER at $h = 0.6$ (a)-(h). The time stamps are indicated in (i), where the legends are the same as in Fig. 11.

filament becomes similar to that of the single filament, e.g., Fig. 4(a). The coupling modes in this category include M3, M5, and M1b. In these modes, the vortices shedding from the adjacent filaments have a rather weak interaction. Nevertheless, the vortex arrangement of each street is still coordinated with that of another street, and this behavior matches the frequency and phase of the filaments.

VI. CONCLUDING REMARKS

The flow-structure interaction of three parallel and evenly spaced filaments in a uniform flow has been studied using a modified penalty immersed-boundary method coupled with a lattice-Boltzmann method and is accompanied by a previously developed linear stability analysis. The flapping modes of the filaments, characteristics of the flow-structure interaction, and vortex structures in the wake are investigated for a range of separation distances between the filaments. At constant Reynolds number, mass ratio, and bending rigidity, we have found that there exist six distinct coupling modes whose appearance depends on the distance between the filaments. These modes include the in-phase mode, symmetrical mode, out-of-phase mode, half-frequency mode, irrational-frequency mode, and erratic flapping. The flapping amplitude, frequency, phase delay, drag, and mechanical energy of the filaments have been characterized for each coupling mode. Moreover, we have also identified four typical vortex structures in the wake, including the coalesced vortices, symmetrical vortices, erratic vortices, and independent vortex streets that are associated with the coupling modes of the filaments. These vortex structures are closely related to the vibratory features of the corresponding coupling modes. Comparing the present numerical simulations with linear theory, we have noticed that some of the coupling modes cannot be predicted by a perturbation analysis where the vibration amplitude is assumed to be small and the frequency to be constant. These additional modes include the half-frequency, irrational-frequency, and erratic flapping modes, and they contain non-identical and/or time-varying frequencies resulting from the nonlinear interaction of the vortices shedding from the filaments.

As the Reynolds number, mass ratio, or the bending rigidity of the filaments varies, the mode spectrum of the filament system may change with some of the modes disappearing and/or re-arranging. Consequently, the filaments at the fixed distance may change from one coupling mode to another, accompanied by the change of the energy level of the filaments.

Comparing the present study with $n=3$ and previous studies of $n=2$, we see that in the case of multiple filaments, each filament can behave quite differently than the other filaments, especially in the nonlinear regime, due to the non-equivalence of their spatial positions. Based on the current result, we expect that for $n>3$, the wake interaction among the filaments with $h=O(1)$ or less is likely to cause complex nonlinear coupling modes in which the filaments have different flapping amplitudes, phases, and frequencies between each other. For example, some of the linear modes[30] such as the symmetrical mode with an odd n may become unstable in the nonlinear regime and develop new modes, and erratic flapping will still exist and will take a more complex form. However, the exact patterns of these nonlinear modes cannot be predicted from the current study.

ACKNOWLEDGMENTS

We would like to acknowledge the grant support from the NSF (No. CBET-0954381) and the Chinese NSFC (No. 10832010) and CAS (No. KJCX2-YW-L05). We are also grateful that one anonymous reviewer pointed out the similarity between the two in-phase modes.

APPENDIX: LINEAR STABILITY ANALYSIS

Linear analysis of multiple filaments in side-by-side arrangement has been established previously by Schouveiler and Eloy[29] and Michelin and Llewellyn Smith.[30] The in-phase, symmetrical, and out-of-phase modes reported here have been reported and discussed extensively in their work. The approach in Schouveiler and Eloy[29] is included here to facilitate the comparison with the numerical simulation. It should be pointed out that the approach in Michelin and Llewellyn Smith[30] provides a more accurate account of the system behavior as they incorporated the effects of the finite length of the filament and the wake.

Here, the filaments are assumed to be infinitely long and the fluid viscosity is neglected, and thus the boundary conditions of the leading- and trailing-ends of the filaments are not taken into account.[29] The three filaments divide the flow field into four regions, as shown in Fig. 1, where φ_j is the velocity potential of the jth region and η_j is the deflection of the jth filament. With the inviscid flow assumption, the potential and velocity are governed by

$$\nabla^2\varphi_j = 0, \quad \mathbf{u}_j = \nabla\varphi_j, \tag{A1}$$

where $\mathbf{u}_j$ is the velocity vector of the jth flow region. The deflection of the jth filament, η_j, is governed by the linearized Euler-Bernoulli beam equation,

$$S\frac{\partial^2\eta_j}{\partial t^2} + U^{-2}\frac{\partial^4\eta_j}{\partial x^4} = \Delta p_j, \tag{A2}$$

where Δp_j is the pressure jump across the filament, $\Delta p_j = p_{j+1} - p_j$. The pressure p_j in the fluid is obtained through the linearized Bernoulli equation,

$$p_j = -\left(\frac{\partial}{\partial t} + \frac{\partial}{\partial x}\right)\varphi_j. \tag{A3}$$

The zeroth-order solution of Eq. (8) is $\mathbf{u}_j = (1,0)$. Using the perturbation analysis, the following governing equation and boundary conditions for the first-order solution can be obtained,

$$\begin{aligned}
&\nabla^2\varphi_j = 0, \quad j = 1,2,3,4,\\
&\frac{\partial\varphi_j(x,h,t)}{\partial y} = \left(\frac{\partial}{\partial t} + \frac{\partial}{\partial x}\right)\eta_1, \quad j = 1,2,\\
&\frac{\partial\varphi_j(x,0,t)}{\partial y} = \left(\frac{\partial}{\partial t} + \frac{\partial}{\partial x}\right)\eta_2, \quad j = 2,3,\\
&\frac{\partial\varphi_j(x,-h,t)}{\partial y} = \left(\frac{\partial}{\partial t} + \frac{\partial}{\partial x}\right)\eta_3, \quad j = 3,4,\\
&\varphi_1(x,\infty,t) = 0, \quad \varphi_4(x,-\infty,t) = 0.
\end{aligned} \tag{A4}$$

To perform linear instability analysis, the velocity potential and the filament deflection are expressed in the form $\varphi_j = \varphi_{0j}(y)e^{i(\omega t+kx)}$ and $\eta_j = \eta_{0j}e^{i(\omega t+kx)}$, respectively, where

ω is the complex frequency, k is the wavenumber of the perturbation, η_{0j} is the amplitude, and $\varphi_{0j}(y)$ is the eigenfunction. Substituting these expressions into Eq. (A4) and following the procedure for the corresponding problem of two side-by-side filaments,[24] it is straightforward to obtain

$$\mathbf{M}\cdot\boldsymbol{\eta} = \begin{pmatrix} a & c & 0 \\ c & b & c \\ 0 & c & a \end{pmatrix} \begin{pmatrix} \eta_{01} \\ \eta_{02} \\ \eta_{03} \end{pmatrix} = 0, \tag{A5}$$

where $\mathbf{M}$ and $\boldsymbol{\eta}$ are the corresponding matrix and vector, $a = -S\omega^2 + U^{-2}k^4 - e^{kh}c$, $b = -S\omega^2 + U^{-2}k^4 - e^{kh}c - e^{-kh}c$, and $c = (\omega + k)^2 k^{-1}\sinh^{-1}(kh)$. In order for η_{0j} to have a nontrivial solution, the determinant of the matrix in Eq. (A5) must be zero, i.e., $|\mathbf{M}| = 0$, which gives the dispersion relation between ω and k.

As $h \to \infty$, it is expected that the filaments become independent of each other and are thus decoupled. In that case, we have $a = b$, $c = 0$, and the dispersion relation for each filament becomes[9]

$$(\omega + k)^2 + (S\omega^2 k - U^{-2}k^5)/2 = 0. \tag{A6}$$

[1] S. Childress, *Mechanics of Swimming and Flying* (Cambridge University Press, New York, 1981).
[2] R. M. Alexander, *Principles of Animal Locomotion* (Princeton University Press, New Jersey, 1993).
[3] J. C. Liao, D. N. Beal, G. V. Lauder, and M. S. Triantafyllou, "Fish exploiting vortices decrease muscle activity," Science **302**, 1566 (2003).
[4] D. N. Beal, F. S. Hover, M. S. Triantafyllou, J. C. Liao, and G. V. Lauder, "Passive propulsion in vortex wakes," J. Fluid Mech. **549**, 385 (2006).
[5] J. D. Eldredge and D. Pisani, "Passive locomotion of a simple articulated fish-like system in the wake of an obstacle," J. Fluid Mech. **607**, 279 (2008).
[6] J. Zhang, S. Childress, A. Libchaber, and M. Shelley, "Flexible filaments in a flowing soap film as a model for one-dimensional flags in a two-dimensional wind," Nature **408**, 835 (2000).
[7] Y. Watanabe, S. Suzuki, M. Sugihara, and Y. Sueoka, "An experimental study of paper flutter," J. Fluids Struct. **16**, 529 (2002).
[8] B. I. Epureanu, L. S. Tang, and M. P. Païdoussis, "Coherent structures and their influence on the dynamics of aeroelastic panels," Int. J. Non-Linear Mech. **39**, 977 (2004).
[9] M. Shelley, N. Vandenberghe, and J. Zhang, "Heavy flags undergo spontaneous oscillations in flowing water," Phys. Rev. Lett. **94**, 094302 (2005).
[10] C. Eloy, C. Souilliez, and L. Schouveiler, "Flutter of a rectangular plate," J. Fluids Struct. **23**, 904 (2007).
[11] C. Eloy, R. Lagrange, C. Souilliez, and L. Schouveiler, "Aeroelastic instability of cantilevered flexible plates in uniform flow," J. Fluid Mech. **611**, 97 (2008).
[12] C. Y. Bao, C. Tang, X. Z. Yin, and X. Y. Lu, "Flutter of finite-span flexible plates in uniform flow," Chin. Phys. Lett. **27**, 064601 (2010).
[13] M. Argentina and L. Mahadevan, "Fluid-flow-induced flutter of a flag," Proc. Natl. Acad. Sci. U.S.A. **102**, 1829 (2005).
[14] L. Zhu and C. S. Peskin, "Simulation of a flapping flexible filament in a flowing soap film by the immersed boundary method," J. Comput. Phys. **179**, 452 (2002).
[15] B. S. H. Connell and D. K. P. Yue, "Flapping dynamics of a flag in a uniform stream," J. Fluid Mech. **581**, 33 (2007).
[16] S. Alben, "The flapping-flag instability as a nonlinear eigenvalue problem," Phys. Fluids **20**, 104106 (2008).
[17] S. Alben and M. Shelley, "Flapping states of a flag in an inviscid fluid: Bistability and the transition to chaos," Phys. Rev. Lett. **100**, 074301 (2008).
[18] L. Huang, "Flutter of cantilevered plates," J. Fluids Struct. **9**, 127 (1995).
[19] S. Michelin, S. G. Llewellyn Smith, and B. J. Glover, "Vortex shedding model of a flapping flag," J. Fluid Mech. **617**, 1 (2008).
[20] C. Lemaitre, P. Hémon, and E. de Langre, "Flutter of cantilevered plates," J. Fluids Struct. **20**, 913 (2005).
[21] I. D. Abrahams, "Acoustic scattering by a finite nonlinear elastic plate II. Coupled primary and secondary resonances," Proc. R. Soc. London, Ser. A **418**, 247 (1988).
[22] N. Peake, "On the unsteady motion of a long fluid-loaded elastic plate with mean flow," J. Fluid Mech. **507**, 335 (2004).
[23] L. D. Landau and E. M. Lifshitz, *Fluid Mechanics* (Pergamon, New York, 1987).
[24] L. B. Jia, F. Li, X. Z. Yin, and X. Y. Yin, "Coupling modes between two flapping filaments," J. Fluid Mech. **581**, 199 (2007).
[25] L. Zhu and C. S. Peskin, "Interaction of two flapping filaments in a flowing soap film," Phys. Fluids **15**, 1954 (2003).
[26] D. J. J. Farnell, T. David, and D. C. Barton, "Coupled states of flapping flags," J. Fluids Struct. **19**, 29 (2004).
[27] L. Tang and M. P. Païdoussis, "The coupled dynamics of two cantilevered flexible platesinaxialflow," J. Sound Vib. **323**, 790 (2009).
[28] S. Alben, "Wake–mediated synchronization and drafting in coupled flags," J. Fluid Mech. **641**, 489 (2009).
[29] L. Schouveiler and C. Eloy, "Coupled flutter of parallel plates," Phys. Fluids **21**, 081703 (2009).
[30] S. Michelin and S. G. Llewellyn Smith, "Linear stability analysis of coupled parallel flexible plates in an axial flow," J. Fluids Struct. **25**, 1136 (2009).
[31] F. B. Tian, H. Luo, L. Zhu, and X. Y. Lu, "Interaction between a flexible filament and a downstream rigid body," Phys. Rev. E **82**, 026301 (2010).
[32] F. B. Tian, H. Luo, L. Zhu, J. C. Liao, and X. Y. Lu, "An immersed boundary-lattice Boltzmann method for elastic boundaries with mass," J. Comput. Phys. **230**, 7266 (2011).
[33] Z. L. Guo, C. G. Zheng, and B. C. Shi, "Discrete lattice effects on the forcing term in the lattice Boltzmann method," Phys. Rev. E **65**, 046308 (2002).
[34] S. Chen and G. D. Doolen, "Lattice Boltzmann method for fluid flows," Annu. Rev. Fluid Mech. **30**, 329 (1998).
[35] C. K. Aidun and J. R. Clausen, "Lattice-Boltzmann method for complex flows," Annu. Rev. Fluid Mech. **42**, 439 (2010).
[36] D. Yu, R. Mei, and W. Shyy, "A multi-block lattice Boltzmann method for viscous fluid flows," Int. J. Numer. Methods Fluids **39**, 99 (2002).
[37] Y. Kim and C. S. Peskin, "Penalty immersed boundary method for an elastic boundary with mass," Phys. Fluids **19**, 053103 (2007).
[38] X. Shi and N. Phan-Thien, "Distributed Lagrange multiplier/fictitious domain method in the framework of lattice Boltzmann method for fluid–-structure interactions," J. Comput. Phys. **206**, 81 (2005).
[39] W. X. Huang, S. J. Shin, and H. J. Sung, "Simulation of flexible filaments in a uniform flow by the immersed boundary method," J. Comput. Phys. **226**, 2206 (2007).
[40] Y. Liu, R. M. C. So, Y. L. Lau, and Y. Zhou, "Numerical studies of two side-by-side elastic cylinders in a cross-flow," J. Fluids Struct. **15**, 1009 (2001).
[41] S. Kim, W. X. Huang, and H. J. Sung, "Constructive and destructive interaction modes between two tandem flexible flags in viscous flow," J. Fluid Mech. **661**, 511 (2010).
[42] G. K. Batchelor, *An Introduction to Fluid Dynamics* (Cambridge University Press, Cambridge, 1967).
[43] J. Z. Wu, H. Y. Ma, and M. D. Zhou, *Vorticity and Vortex Dynamics* (Springer-Verlag, Berlin, 2006).